

Supplementary Information

Phase Synchronization of two anharmonic NEMS oscillators

M. H. Matheny, M. Grau, L. G. Villanueva, R. B. Karabalin, M. C. Cross, M. L. Roukes

*Kavli Nanoscience Institute and Departments of Physics, Applied Physics, and Bioengineering,
California Institute of Technology, Pasadena, California 91125*

I. Theoretical derivation of synchronization equations for two anharmonic oscillators

We start with the slow time equation[1] for two oscillators with two feedback[2, 3] terms: one which is common to both oscillators (f_c), and one that affects the corresponding oscillator only (f_i , $i=1,2$). These are

$$\frac{d\tilde{A}_1}{dT} - i\left(\frac{\delta_1}{2} + \lambda_{11}|\tilde{A}_1|^2\right)\tilde{A}_1 + \frac{\tilde{A}_1}{2} = f_1(\tilde{A}_1) + f_c(\tilde{A}_1, \tilde{A}_2), \quad (\text{S.I.1})$$

and

$$\frac{d\tilde{A}_2}{dT} - i\left(\frac{\delta_2}{2} + \lambda_{22}|\tilde{A}_2|^2\right)\tilde{A}_2 + \frac{\tilde{A}_2}{2} = f_2(\tilde{A}_2) + f_c(\tilde{A}_2, \tilde{A}_1) \quad (\text{S.I.2})$$

where $\delta_{1,2} = Q\left(\frac{\omega_{1,2}^2}{\omega_0^2} - 1\right)$ defines the offset of the natural resonance frequency of each NEMS device $\omega_{1,2}$ to a nearby frequency, ω_0 , $\tilde{A} = \tilde{a}e^{i\varphi}$ is the complex slow time oscillator displacement, and the nonlinear coefficient λ is the relationship of the device displacement to the relative change in the NEMS resonance frequency (there is a factor of 3/8 that has been folded into this constant with respect to references 1 and 2). The terms $f_{1,2}$ and f_c are the ‘‘oscillator feedback’’ and ‘‘coupling signal’’ in Figure 1, respectively. For a saturated oscillator feedback with linear, reactive, diffusive coupling these equations become

$$\frac{d\tilde{A}_1}{dT} - i\left(\frac{\delta_1}{2} + \lambda_{11}|\tilde{A}_1|^2\right)\tilde{A}_1 + \frac{\tilde{A}_1}{2} = \frac{s}{2}e^{i\varphi_1} + i\frac{\beta}{2}(\tilde{A}_2 - \tilde{A}_1), \quad (\text{S.I.3})$$

and

$$\frac{d\tilde{A}_2}{dT} - i\left(\frac{\delta_2}{2} + \lambda_{22}|\tilde{A}_2|^2\right)\tilde{A}_2 + \frac{\tilde{A}_2}{2} = \frac{s}{2}e^{i\varphi_2} + i\frac{\beta}{2}(\tilde{A}_1 - \tilde{A}_2), \quad (\text{S.I.4})$$

where s is the level of the saturation, and β is the (real-valued) strength of the coupling.

The magnitude of oscillation can be scaled by the saturation s ($\tilde{A} = A * s$), which yields

$$\frac{dA_1}{dT} - i\left(\frac{\delta_1}{2} + \lambda_{11}s^2|A_1|^2\right)A_1 + \frac{A_1}{2} = \frac{1}{2}e^{i\varphi_1} + i\frac{\beta}{2}(A_2 - A_1), \quad (\text{S.I.5})$$

and

$$\frac{dA_2}{dT} - i\left(\frac{\delta_2}{2} + \lambda_{22}s^2|A_2|^2\right)A_2 + \frac{A_2}{2} = \frac{1}{2}e^{i\varphi_2} + i\frac{\beta}{2}(A_1 - A_2). \quad (\text{S.I.6})$$

We combine the terms $\lambda_{11}s^2$ into a single term α , which is the nonlinear frequency pulling[4].

Equations S.I.5 and S.I.6 can be separated into magnitude and phase,

$$\frac{da_1}{dT} = -\frac{a_1}{2} + \frac{1}{2} + \text{Re}\left(i\frac{\beta}{2}(a_2e^{i(\varphi_2-\varphi_1)} - a_1)\right), \quad (\text{S.I.7})$$

$$\frac{da_2}{dT} = -\frac{a_2}{2} + \frac{1}{2} + \text{Re}\left(i\frac{\beta}{2}(a_1e^{i(\varphi_1-\varphi_2)} - a_2)\right), \quad (\text{S.I.8})$$

$$\frac{d\varphi_1}{dT} = \frac{\delta_1}{2} + \alpha a_1^2 + \text{Im}\left(i\frac{\beta}{2}\left(\frac{a_2}{a_1}e^{i(\varphi_2-\varphi_1)} - 1\right)\right), \quad (\text{S.I.9})$$

and

$$\frac{d\varphi_2}{dT} = \frac{\delta_2}{2} + \alpha a_2^2 + \text{Im} \left(i \frac{\beta}{2} \left(\frac{a_1}{a_2} e^{i(\varphi_1 - \varphi_2)} - 1 \right) \right). \quad (\text{S.I.10})$$

To examine synchronized states we look at the oscillator phase difference $\varphi = \varphi_2 - \varphi_1$. Equations S.I.7-S.I.10 become

$$\frac{da_1}{dT} = -\frac{a_1}{2} + \frac{1}{2} - \frac{\beta}{2} a_2 \sin \varphi, \quad (\text{S.I.11})$$

$$\frac{da_2}{dT} = -\frac{a_2}{2} + \frac{1}{2} + \frac{\beta}{2} a_1 \sin \varphi, \quad (\text{S.I.12})$$

and

$$\frac{d\varphi}{dT} = \frac{d\varphi_2}{dT} - \frac{d\varphi_1}{dT} = \frac{\delta_2}{2} - \frac{\delta_1}{2} + \alpha a_2^2 - \alpha a_1^2 + \frac{\beta}{2} \left(\frac{a_1}{a_2} - \frac{a_2}{a_1} \right) \cos \varphi. \quad (\text{S.I.13})$$

These are equations 1,2, and 3 from the main text where the prime character ‘ represents the derivative with respect to slow time T , and $\frac{\delta_2}{2} - \frac{\delta_1}{2} = \Delta\omega$.

II. Experimental Methods

Experimental Methods: Device fabrication has been previously described by Villanueva *et al*[2]. All measurements were taken at a pressure of less than 100mT through a balanced bridge technique (not pictured in the figure)[5] in order to reduce the effect of parasitic capacitances[3]. All three synchronization parameters are modified by external and independent DC voltage sources. The coupling strength can be controlled by adjusting the feedback gain in the coupling loop. We amplify and tune (using the red DC control voltage box in Figure 1 of main text) a voltage controlled attenuator (double-line box in Figure 1 of main text) in order to modify this coupling

feedback gain. The frequency difference between the two oscillators can be linearly controlled by inducing stress in one of the beams by a DC piezovoltage, as shown by the blue box in Figure 1. The frequency pulling can be adjusted by varying the absolute oscillator amplitudes (keeping the relative amplitudes fixed to ensure that Equations 1-3 remain valid) through the use of the voltage controlled attenuators (single-line dark box controlled by green DC voltage). The amplifiers used in the setup were tested at each stage to ensure linearity of signal transfer. For more information see Supplementary Information section III. All data (except for phase noise) are taken by two separate spectrum analyzers so that amplitude and frequency can be measured independently for the two oscillators. Phase noise is measured on a single spectrum analyzer with a phase noise module, with the input switched for either oscillator. Simulations (Figure 3) of the basins of attraction were carried out in Matlab, and the linear stability analysis was carried out in Mathematica.

III. Experimental resonator properties

The devices were selected such that the parameters were nearly identical. In Table S.1 we show the values for the resonator frequency and quality factor. We have published more details elsewhere[3]. Note that throughout the quality factors and frequencies varied ~6% from device heating due to piezoresistive bias.

Parameter	Device “1”	Device “2”
Frequency, f_0	13.056 MHz	13.060 MHz
Q factor	1640 ± 70	1680 ± 100

In Figure
show the

Table S.1. Fit parameters of the resonance plots shown below. The uncertainties in Q are found from measuring Q at different times throughout the experiment.

S.1 we
driven

response from which the values of Table S1 are found. The devices came from the same fabrication run and design.

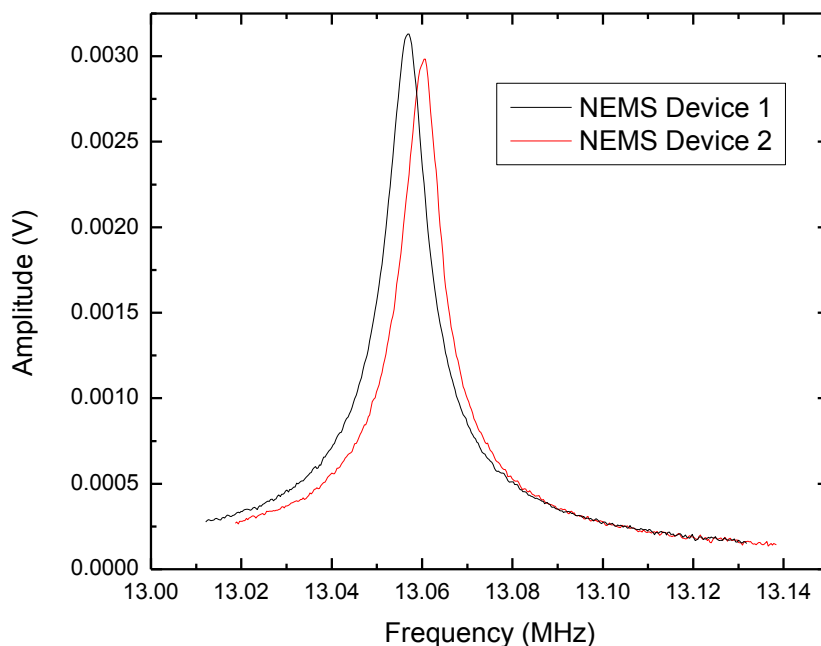


Figure S.1: Driven response of the two devices. Note the similarity in frequency and quality factor.

IV. Calibration of setup, and measurement of synchronization parameters

Before calibrating the three synchronization parameters $(\Delta\omega, \alpha, \beta)$, we must ensure that both the “oscillator” and “coupling” feedback signals (see Figure 1 of the main text) have the proper phase shifts, i.e., $f_{1,2}$ is purely dissipative and f_c is purely reactive in equations S.I.1 and S.I.2. If the oscillators are uncoupled, the proper phase shift in the “oscillator” feedback loops causes maximum oscillation. At low saturation, the oscillator magnitude is a Lorentzian[3] function with respect to the frequency. In the slow time, this is

$$|\tilde{A}|^2 \propto \frac{s^2}{1 + 4\Omega^2}, \quad (\text{S.II.1})$$

with $\Omega = \frac{d\varphi_{1,2}}{dt}$ from equations S.I.9 and S.I.10. We measure the oscillation amplitude and frequency as the phase shift in the oscillator loop is varied. We plot this for oscillator 1 in Figure S.2(a). A Lorentzian fit of this data yields the proper setting for the voltage controlled phase shifter embedded in the oscillator loop (the voltage controlled phase shifter is not pictured in Figure 1 from the main text). From the Lorentzian fit, the central frequency gives us the proper setting for the phase shifter, as shown in figure S.2(b).

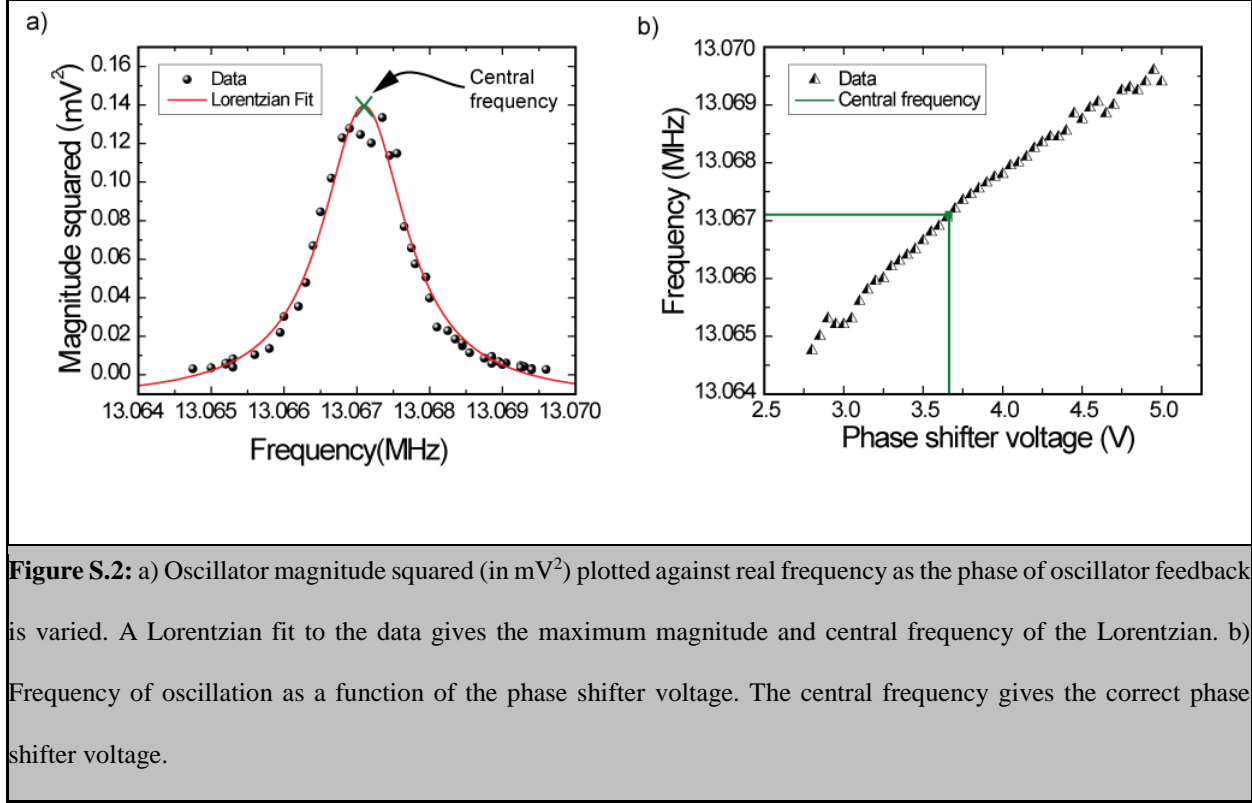


Figure S.2: a) Oscillator magnitude squared (in mV²) plotted against real frequency as the phase of oscillator feedback is varied. A Lorentzian fit to the data gives the maximum magnitude and central frequency of the Lorentzian. b) Frequency of oscillation as a function of the phase shifter voltage. The central frequency gives the correct phase shifter voltage.

A. Calibration of coupling, β

In order to verify that the coupling loop is purely reactive, we compare two different measurements: 1) the level of amplification of the signal from the NEMS device through the coupling loop, and 2) the frequency shifts of the two oscillators due to the coupling feedback. Note that if the coupling is not strictly reactive, then according to reference 3, we must include a dissipative term to the feedback,

$$f_c(A_1, A_2) = (K + i\beta)(A_2 - A_1). \quad (\text{S.II.2})$$

From figure 1 in the main text, if we turn off the second oscillator, then S.II.2 gives

$$f_c(A_1, A_2) = (K + i\beta)(-A_1). \quad (\text{S.II.3})$$

The feedback described in equation S.II.3, when inserted into equation S.I.5, will lead to not only tuning of the oscillator by $-\beta/2$, but also additional dissipation proportional to K . Note that the magnitude $|K + i\beta|$ is the total gain of a signal through the coupling loop. By measuring this coupling loop gain and comparing it to measurements of the oscillator frequency shift, we can verify that $|K + i\beta| = |\beta|$, i.e., our coupling is strictly reactive. In Figure S.3, $|K + i\beta|$ is measured by the first method (red line, right vertical axis), and β is measured using the frequency shift of the two oscillators (blue stars and green circles, left vertical axis). If the red line had a larger magnitude than the data points from the frequency shifts, then there would be a dissipative component to the feedback ($K \neq 0$). However, these two measurements agree. These measurements not only verify that the coupling feedback has the proper phase shift, but also provide a calibration for coupling β in terms of the voltage of the coupling attenuator.

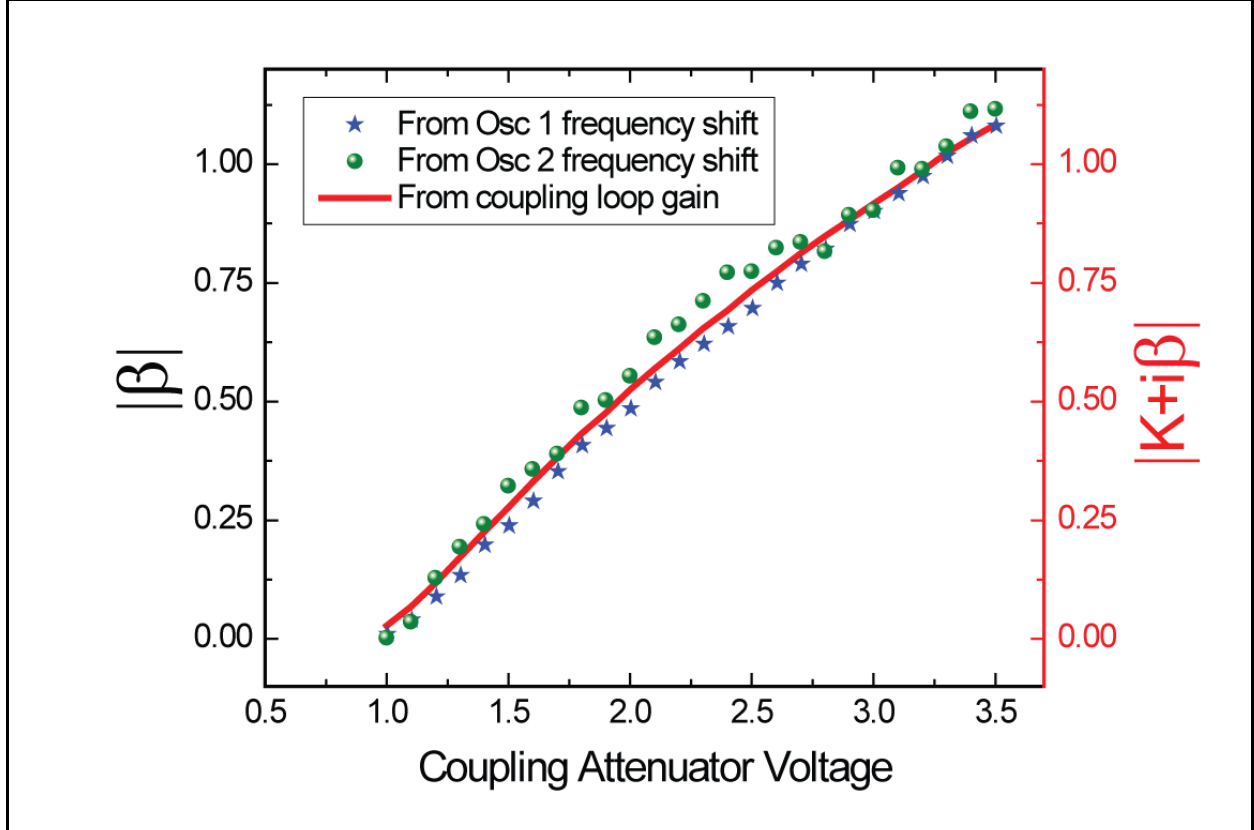


Figure S.3. Different measurements to calibrate coupling. The green (blue) points are found using tuning data from oscillator 1 (2), and correspond to the left vertical axis. The red curve is found by measuring gain around the coupling loop; it corresponds to the right vertical axis.

B. Calibration of frequency pulling, α

In order to calibrate the frequency pulling $\alpha = \lambda s^2$, we first calibrate the NEMS displacement and oscillator magnitude $|\tilde{A}|$. The thermomechanical noise of the NEMS device provides an absolute scale by which we can calibrate the device displacement from the electronic signal[2]. We can scale the NEMS displacement to the oscillator magnitude. With the oscillator and coupling feedback turned off, we measure the frequency response of the NEMS device under a constant level of external excitation. Fitting the NEMS frequency at the peak magnitude, for different values of excitation, yields the nonlinear coefficient λ [6]. hen the oscillators are uncoupled, the maximum

oscillator amplitude corresponds to the level of saturation s (equation S.I.3 and S.I.4). Changes to the feedback saturation level, and thus the nonlinear pulling, can be made by adjusting the oscillator loop's attenuator after the limiting diode, as diagrammed in Figure 1 of the main text.

C. Calibration of detuning, $\Delta\omega$

We present two different ways of measuring the detuning $\Delta\omega$. When detuning is held fixed, a low value of coupling β in equations S.I.11-S.I.13 yields a phase equation

$$\frac{d\varphi}{dT} = \Delta\omega + \alpha a_2^2 - \alpha a_1^2 = \Delta\omega. \quad (\text{S.II.4})$$

According to equation S.II.4, we can find the fixed detuning by measuring the oscillator frequency difference at zero coupling.

However, when the detuning is swept, a different calibration method is needed. In the experiment, we measure the oscillator frequency difference as a function of a piezoelectric tuning voltage (which changes the stress in one of the devices and hence the detuning[7]). We wish to make a correspondence between this tuning voltage and the detuning $\Delta\omega$. When the oscillators are far from the synchronization regime, the detuning dominates the other terms on the right hand side of equation S.I.13, so the oscillator frequency difference is proportional to the detuning. A linear fit to data far from the synchronized regime provides a relationship between the piezoelectric tuning voltage and the oscillator frequency difference. We therefore calibrate the detuning in terms of the piezoelectric tuning voltage by means of the oscillator frequency difference at data points far from synchronization. The calibration takes advantage of the fact

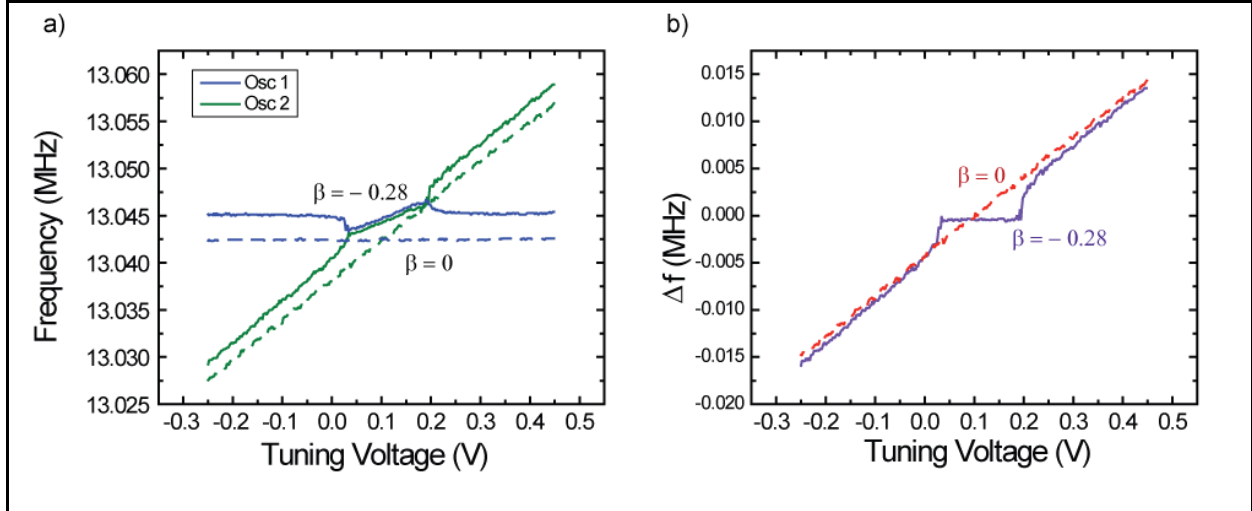


Figure S.4: a) Raw data of sweeps of detuning under different coupling conditions (dashed lines $\beta = 0$, solid lines $\beta = -0.28$), with each sweep taking minutes. The synchronization region appears when coupling is turned on. The two sweeps, taken hours apart, show that the NEMS device frequencies are drifting. b) Difference in frequency for the same sweeps. Straight lines are fit to the end sections of (b) in order to calibrate $\Delta\omega$ and correct for drifts.

that the detuning is linear in the piezoelectric tuning voltage[8]; we can interpolate each linear fit and calibrate the detuning in the synchronization regime. In figure S.4 (a), we show the raw data for the frequencies of the two oscillators from two sweeps with different coupling. In Figure S.4 (b), for the same sweeps, we show the (unscaled) oscillator frequency differences, where the linear fits are performed.

The time between the measurements for the two different values of coupling \sim hours, thus allowing drifts in oscillator frequencies to set in. However, the drift within each sweep is small, given that each sweep \sim minutes. Therefore, through the method outlined above, each sweep can be calibrated to correct for these drifts.

Note that in Figure S.4 (a), with the coupling turned on, there is *mutual* entrainment, evidence that our coupling is symmetric. Adler's equation (equation 4 from the main text) originally described[9] an experiment where oscillator 1 is fed the signal of oscillator 2, but oscillator 2 is

not fed the signal of oscillator 1. This asymmetric coupling led to oscillator 1, the “slave” oscillator, being dominated by oscillator 2, the “master” oscillator. In our experiment, it is clear that both oscillator frequencies shift towards one another, i.e., each oscillator has equal influence over the final state.

V. Notes on the phase noise measurement

The phase noise data was taken on an Agilent N9030 PXA signal analyzer using the “phase noise” mode. The noise data (60 points) surrounding the 1 kHz offset was fit to a straight line (in a log plot) and the 1 kHz point was interpolated. The error is the uncertainty in a least squares fit of the data. The upper horizontal line of this plot is the average noise between the two oscillators taken at lowest coupling. The lower horizontal line is the average taken at highest coupling.

In the experiment, the oscillator phase noise is vastly different in the configuration shown for Figures 2 and 3 of the main text. When synchronization occurs in this setting, one oscillator dominates the noise of both when synchronized. However, if the phase delay of the oscillator feedback loops are adjusted, the phase noise of the two oscillators can be adjusted[3]. We adjust the feedback phase delay so that the phase noises are equivalent. Inevitably, a more general form of equations presented in Section I from the main text must be considered, and the values for alpha and delta omega cannot be calibrated as outlined in Section III. However, the coupling loops are not changed, and is very small and mutually symmetric, and so the overall behavior follows two simple phase oscillators. We therefore do not quantify when the synchronization will occur, but can predict the reduction in phase noise for the synchronized oscillators.

VI. Previous works on synchronization

A. Definition of synchronization

The widely accepted definition of synchronization is given in the text “Synchronization: A universal concept in nonlinear science” by Pikovsky, Rosenblum, and Kurths[10] on page 8 of the introduction:

“We understand synchronization as an **adjustment of rhythms of oscillating objects due to their weak interaction.**” (*emphasis theirs*)

They later expand on the concept of “weak interaction” on page 17:

“..we can say that the introduction of coupling should not qualitatively change the behavior of either one of the interacting systems and should not deprive the systems of their individuality.”

And later on the same page:

“To call a phenomenon synchronization, we must be sure that:

- We analyse the behavior of two self-sustained oscillators, i.e. systems capable of generating their own rhythms;
- The systems adjust their rhythm due to a weak interaction;

- The adjustment of rhythms occurs in a certain range of systems' mismatch; in particular, if the frequency of one oscillator is slowly varied, the second follows this variation.

Correspondingly, a single observation is not sufficient to conclude synchronization.

Synchronization is **a complex dynamical process, not a state.**" (*emphasis theirs*).

We examine the previous claims of synchronization with this definition.

B. Previous claims of mechanical synchronization

We know of two prior claims of synchronization in miniaturized mechanical systems[11, 12].

These claims are examined in more detail in the following sections.

a. Shim, et al. Science 2007

Shim, *et al.* claimed to observe the synchronization of a pair of coupled nanomechanical oscillators. However, that work studied a pair of coupled nanomechanical resonators driven by an external periodic signal and measured the response amplitude at the drive frequency or at a harmonic of the drive frequency. They did not give any experimental or theoretical evidence for self-sustained oscillations. The system which was under study had very strong coupling with the two linked beams always phase coherent. This study is analogous to a pair of pendulums with a rigid bar connecting the pendulum bobs, and driven with a harmonic force.

b. Zhang, et al. PRL 2012

The configuration of the optomechanical system presented in Zhang, *et al.* is not capable of the weak coupling needed to establish synchronization. This is demonstrated both experimentally, and in the modeling. The authors also misinterpret a key piece of data. All figures mentioned in this section refer to the figures in Zhang, *et al.*

These authors performed their experiment by coupling two optomechanical oscillators together by their evanescent light fields. Before coupling them together, they confirmed their devices are individually oscillating, as shown Figures 3 a,b. Later, in Figures 3 c,d,e, they coupled the optical cavities together into symmetric and anti-symmetric normal modes, and excited the system through one device. This serves both to excite two oscillators simultaneously, with only one optical input and to couple the devices together.

The data in their Figure 3 show the system does not in fact have weak coupling. Figure 3 c,d,e shows the coupled system under three different values of laser power. Since an increase in the laser power is associated with an increase in the optical coupling between the two devices, Figure 3c is the data for the smallest coupling, and so if the system is strongly coupled in Figure 3c, the rest of the data is also strongly coupled. With respect to Figure 3c, the authors stated that the left optomechanical oscillator (L OMO) started self-sustained oscillation at the white dashed line. At a stronger laser detuning (~ 0.23 GHz), the right optomechanical oscillator (R OMO) started self-sustained oscillation and the L oscillator shut off. This is also found in numerical simulation in Figure 3f. The fact that the oscillation of R OMO shut down L OMO is clear evidence the system was strongly coupled: the self-oscillation of one oscillator should not turn off the other, if they are truly independent and weakly coupled.

The model for the optomechanical system provided in the supplementary information of the study also demonstrates the strong coupling. In section S5.A the authors give equations for the

radiation pressure induced self-oscillation, the optical spring effect, and the reactive and dissipative coupling between the oscillators. The model shows the dissipative coupling between oscillators is comparable to the driving terms of the self-oscillation, regardless of the laser power or detuning. Depending on the sign of the coupling, self-oscillation in one optomechanical device can turn off the other oscillator. This does not constitute weak coupling, since the behavior of the oscillators should not qualitatively change due to the interaction. This system, when the optical cavities are fully coupled into symmetric and anti-symmetric modes, is not capable of weak coupling. A separation of the coupling and the excitation mechanism is necessary for weak coupling a demonstration of synchronization.

The data in Figure 3d appears to show the two oscillations merging into a single oscillation; however, the authors misinterpreted the data in this figure, which does not in fact show evidence of two oscillations. The transition in Figure 3d is also presented in Figure 4 showing the spectra. The unsynchronized behavior in Figure 4d was suggested to show two independent self-sustained oscillations transitioning to a single synchronized state in Figure 4e. Examining the spectral width of the “R” oscillator (blue peak on the left in d) shows it is not consistent with self-sustained oscillation. As Zhang, *et al* pointed out earlier, when uncoupled oscillators are described, “...the optomechanical resonator starts self-sustaining oscillations and becomes an OMO **characterized by sudden linewidth narrowing** and oscillation amplitude growth.” (*emphasis ours*). The spectral width of the blue peak in Figure 4d does not show this narrowing but is, however, consistent with the quoted width of the driven non-self-oscillatory resonance width, determined by the resonant frequency divided by the quality factor. In Figure 4d, the width of the blue peak on the left is approximately.

Also, the oscillations in Figure 3b are of a much different character (amplitude and width) than the one in Figure 3d for the “R” oscillator. It is also surprising, if the coupling was weak, that the two devices began self-oscillation at the same threshold in the coupled case (Figure 3d) when the thresholds were vastly different in the uncoupled case (Figures 3a,b): the authors do not give any explanation for this. We conclude that the publication by Zhang, *et al.* did not show two oscillations transitioning to a single oscillatory state.

C. Josephson Junctions

There are two main features which distinguish our results from those of Josephson Junctions (JJs). Firstly, JJs behave as rotors driven by a constant torque, whereas our system is a more typical representation of standard self-sustained oscillators. Secondly, we have much more control over system parameters.

Josephson Junctions can be likened to a pendulum driven by a constant torque. The frequency of these rotations is a function of the applied torque exerted on the pendulum, which corresponds to an increase in the bias current across the JJ. However, in an oscillator, the frequency is determined by the physical properties of the system, such as pendulum length and gravitational restoring force for the pendulum. Although rotors share some features of self-sustained oscillators, there are important differences and they will not exhibit all the phenomenon found in self-sustained oscillations. Also, in JJs, the onset of the periodic motion is not a supercritical Hopf bifurcation as in simple feedback oscillators, but a saddle-node bifurcation[13].

The current state of the art for Josephson systems does not exhibit the degree of control as demonstrated in our system. Experiments on arrays of Josephson Junctions have demonstrated

control over only the driving current, while we have control over all the parameters in our system. The JJ arrays can indeed be mapped to the Kuramoto model in some limit; however, extending their relevance to oscillator synchronization outside of this limit has not been shown. We have shown (Figure 3 of the main text) synchronization of self-sustained oscillations which do not obey the Kuramoto model. This phenomenon cannot be found in JJs.

D. Spin-Torque Oscillators

Spin-torque oscillators have been shown to synchronize (see Kaka, *et al* 2005[14]), but the system control is limited and there is no match of any theoretical models to the experimental data, in contrast to our study. In Kaka, *et al.* only one parameter was changed, namely, the current, and therefore the frequency. The study had a fixed value of coupling (set by fabrication constraints). The presented implementation also has the disadvantage that changing the current (or the magnetic field) inevitably changes the power and noise properties. On the other hand in our system we can change the frequency independently of amplitude, noise, and coupling.

REFERENCES

- [1] R. Lifshitz, and M. C. Cross, *Nonlinear Dynamics of Nanomechanical and Micromechanical Resonators* (Wiley-VCH Verlag GmbH & Co. KGaA, 2009), Reviews of Nonlinear Dynamics and Complexity.
- [2] L. G. Villanueva *et al.*, *Nano Letters* **11** (2011).
- [3] L. G. Villanueva *et al.*, *arXiv:1210.8075* (2012).
- [4] M. C. Cross *et al.*, *Physical Review E* **73** (2006).
- [5] K. L. Ekinici *et al.*, *Applied Physics Letters* **81** (2002).
- [6] M. Matheny *et al.*, *Nano Lett* (2013).
- [7] R. B. Karabalin *et al.*, *Physical Review Letters* **106** (2011).
- [8] R. Karabalin, (California Institute of Technology, 2008).
- [9] R. Adler, *Proceedings of the IRE* **34** (1946).
- [10] A. Pikovsky, M. Rosenblum, and J. Kurths, *Synchronization : a universal concept in nonlinear sciences* (Cambridge University Press, Cambridge, 2001), The Cambridge nonlinear science series, 12.
- [11] S. B. Shim, M. Imboden, and P. Mohanty, *Science* **316** (2007).
- [12] M. Zhang *et al.*, *Physical Review Letters* **109** (2012).

- [13] S. H. Strogatz, *Nonlinear dynamics and Chaos : with applications to physics, biology, chemistry, and engineering* (Addison-Wesley Pub., Reading, Mass., 1994), Studies in nonlinearity.
- [14] S. Kaka *et al.*, *Nature* **437** (2005).